2025 IEEE/SICE International Symposium on System Integration (SII)
January 21-24, 2025, Munich, Germany

Estimation of the 3D printing filling density effect on natural frequency and damping ratio and the optimal filling density of robot structure

Yuanhao Bao and Takeshi Takaki[1]

Abstract— **In this study, we measured the natural frequency and damping ratio of onyx-material robot arm specimens and obtained the variation law of the Young's modulus and attenuation coefficient with filling density. Based on this, we obtained the equations for estimating the natural frequency and damping ratio of robot arm specimens for any filling density and size. This equation allows estimating its vibration characteristics even without printing the robot arm. Finally, we combined the equations for calculating the natural frequency and damping ratio with those for the settling time and investigated how to determine the optimal filling density under different loads. The results show that the anti-vibration effect of the specimen is the worst for a filling density of 25-30%. Therefore, this filling density should be avoided. We also found that the settling time for a 10% filling density is shorter than that of many specimens with a high filling density. To achieve light weights, a 10% filling density may be an option. The proposed equations and curves can provide guidelines to design a robot arm with anti-vibration effect.**

I. INTRODUCTION

Compared with traditional metal processing, 3D printing requires less time to shape, results in lighter products, and features higher processing freedom. Thus, it is widely used in robot research. In a previous study conducted by Takaki et al. [1], the damping ratio of resin materials like Onyx-FR,Onyx-N was found to be relatively high than metal material A2017. We aim to exploit this advantage of resin materials in the design of a more stable robot arm.

Fused deposition modelling (FDM) 3D printing allows for free setting of filling density. Different filling densities can lead to distinct physical properties even if the materials used are the same. The purpose of this study is to establish optimized filling density design criteria to enhance the anti-vibration capabilities of 3D-printed robotic arms.

Previous studies [2,3] pointed out that for onyx and PLA [4], specimens with higher filling densities feaure higher Young's modulus under the same filling pattern. Evidently, the cross-sectional area will vary with the packing density. Unfortunately, previous studies did not pay attention to this variation, which leads to inaccurate determination of stress and Young's modulus.

In this paper, we observed that Young's modulus and the attenuation coefficient vary with filling density. Therefore, we selected filling density as the design parameter and determined the relationship between filling density and changes in Young's modulus and the attenuation coefficient through experiments and calculations. Using the least squares method, we summarized these relationships in a change equation.

By applying this equation for Young's modulus and the attenuation coefficient in relation to filling density, we estimated the natural frequency and damping ratio of the robot arm for various sizes and filling densities. Finally, we used the proposed equations to estimate the settling time required for the robot arm to transition from vibration initiation to cessation at different filling densities and compared these estimates to corresponding real values.

The results show that the proposed equation to determine the settling time can accurately estimate the vibration duration of the robot arm for different filling densities, thereby helping set the best filling density.

The remainder of this paper is structured as follows. In Section 2, we report on the calculations of the variations in the Young's modulus and propose equations for estimating the natural frequency and damping ratio. In Section 3, we compare the estimated values of natural frequency and damping ratio with the corresponding experimental values. Finally, we discuss and determine the optimal filling density based on the settling time.

II. PRINCIPLE AND CALCULATION

A. Fill density changes the Young's modulus

A robot arm can be regarded as a single-degree-of-freedom cantilever beam model, as shown in Fig. 1. The vibration direction is along the Z-direction, and the vibration of the cantilever beam can be expressed by the following equation [5]:

where w is the deflection of the cantilever beam in the Z-axis direction; λ_i (i=1, 2..., ∞) is a constant under different vibration modes (the constants under the primary and secondary models are 1.875 and 4.694, respectively); and C_i, E_i, and F_i are constants under different vibration models.

$$\begin{aligned} w = \sum_{i=1}^{n} \Big\{ & C_i[(\cosh\lambda_i\frac{x}{l} - \cos\lambda_i\frac{x}{l})(\sinh\lambda_i + \sin\lambda_i) \\ & -(\sinh\lambda_i\frac{x}{l} - \sin\lambda_i\frac{x}{l})(\cosh\lambda_i + \cos\lambda_i)] \Big\} \\ & (E_i\cos\omega_i t + F_i\sin\omega_i t) \end{aligned} \tag{1}$$

Natural Frequency: f_i is the natural frequency under different vibration models, which can be calculated using the Eq. (2):

*This research is subsidized by New Energy and Industrial Technology Development Organization (NEDO) under a project JPNP20016

[1]Yuanhao Bao and Takeshi Takaki are with Graduate School of Advanced Science and Engineering, Hiroshima University, 1-4-1 Kagamiyama, Higashi-Hiroshima, Hiroshima, 739-8527 Japan. takaki@hiroshima-u.ac.jp, baoyuanhao530@gmail.com.

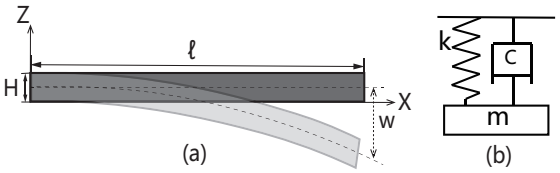

Fig. 1. (a) Cantilever beam model of the robotic arm. (b) Particle model.

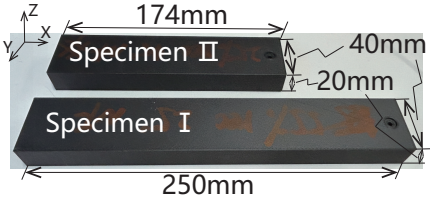

Fig. 2. Specimen for two sizes of robot arms.

TABLE I

The dimensions and natural frequencies of the specimen I (40x20x250 mm) in different filling densities μ

Specimen I						
μ (%)	10	25	40	55	70	100
Mass m (g)	36.5	56.09	78.43	100.4	123.0	166.44
f_i (Hz)	125	105	109	110	111	113
ζ	0.02	0.0303	0.0326	0.0365	0.0363	0.068

$$f_i = \frac{\omega_i}{2\pi} = \frac{\lambda_i^2}{2\pi l^2}\sqrt{\frac{EI_Y}{\rho A}} \tag{2}$$

where ω_i is the natural angular frequency under different vibration models, l is the total length of the cantilever beam,I_Y is the second moment of area, E is Young's modulus of the material at the current fill density, ρ is the material density, and A is the cross-sectional area of the cantilever beam.

Therefore, the product of the Young's modulus E and second moment of area I_Y can be expressed as follows:

$$EI_Y = \frac{4m\pi^2 l^3 fi^2}{\lambda^4} \tag{3}$$

In the equation above, the weight of specimen m is:

$$m = \rho A l \tag{4}$$

As shown in Fig. 2, we measured the natural frequency and damping ratio of two different sizes of robot arm specimens, I and II, under a rectangle filling pattern. The Z-axis direction is the laminate direction. The measurement method is described in detail in the experimental part of Section 3. The dimensions, natural frequency f_i and damping ratio ζ of the specimens for different filling densities μ are shown in Table. I, II.

Given that the cross-sectional dimensions of specimens I and II are the same, the second moment of area I_Y for each filling density remains the same. Theoretically, as long as the variation in the Young's modulus E is stable, the EI_Y values of specimens I and II for each filling density should be the same.

TABLE II

The dimensions and natural frequencies of the specimen II (40x20x174 mm) in different filling densities μ

Specimen II						
μ (%)	10	25	40	55	70	100
Mass m (g)	22.29	36.77	51.20	65.65	80.13	104.53
f_i (Hz)	276	253	261.9	274.1	295.91	319
ζ	0.022	0.0226	0.022	0.0227	0.0209	0.032

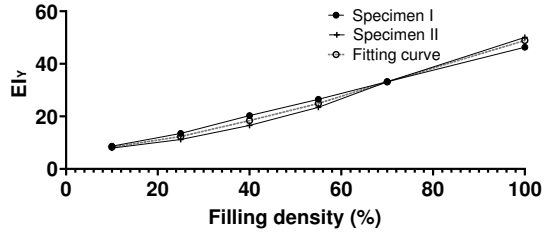

Fig. 3. The EI_Y values of specimens I and II at each filling density.

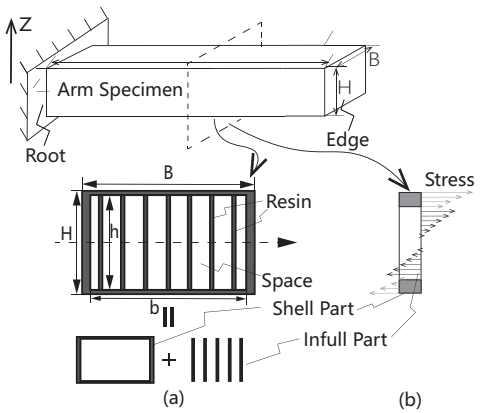

Fig. 4. (a) The cross section of the robot arm specimen. (b) Stress distribution in cross section.

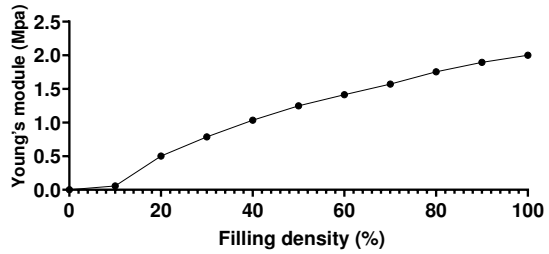

Fig. 5. The Young's module of Onyx in different filling density.

Using Eq. (3), we obtained the EI_Y values of specimens I and II for each filling density; they are shown in Fig. 3. The slopes of the two curves are approximate. We averaged the EI_Y values for each filling density, thereby obtaining the fitting curve represented by the dotted line.

Calculation of the Young's modulus: Fig. 4(a) shows the x-direction cross-section of the robotic arm specimen; B is the section width and H is the section height; b is the width of the inside after removing the shell; and h is the height of the inside after leaving the shell. As shown in Fig. 4(b), given that the filling density of the outer shell is 100% and is different from the filling density of the interior, the

EI_Y value of the cross-section, which encompasses different Young's moduli, can be calculated by the following equation [5][6]:

$$EI_Y = E_s I_s + E_{in} I_{in} = E_s(\frac{BH^3}{12} - \frac{bh^3}{12}) + E_{in}(\mu \frac{bh^3}{12}) \quad (5)$$

Where E_s and E_{in} are the Young's modulus of the shell and filling part, respectively, and I_s and I_{in} are the second moments of the section of the shell and filling part, respectively. The filling density μ ranges from 0 to 1. When $\mu = 0$, the filling density is 0. If $\mu = 1$, the specimen is a solid structure.

The Young's modulus of the shell E_s is equivalent to the Young's modulus at 100% filling density $E_{in100\%}$ equal to 2 Gpa. According to the results obtained from Fig. 3 and Eq. (5), the Young's modulus E_{in} of the resin for each filling density can be gradually obtained, as shown in Fig. 5.

B. Estimating natural frequency

We used the data showing the variation of Young's modulus E with filling density μ in Fig. 5 and obtained the equation for the curve in Fig. 5 by applying the least squares method in Microsoft Excel. The increasing trend of Young's modulus E can be expressed by Eq. (6).

$$E_{in} = -1.47\mu^2 + 3.67\mu - 0.22 \quad (0.1 \leq \mu \leq 1) \quad (6)$$

By combining Eqs. (5), (6) and (3), we can obtain Eq. (7) and use it to calculate the natural frequency of the specimen for any size and values of filling density ranging from 10% to 100%.

$$f_i = J\sqrt{\frac{E_s(\frac{BH^3}{12} - \frac{bh^3}{12}) + (-1.47\mu^2 + 3.67\mu - 0.22)(\mu \frac{bh^3}{12})}{m}} \quad (7)$$

In the equation above,

$$J = \frac{\lambda^2}{2\pi l^{\frac{3}{2}}}$$

C. Fill density changes the attenuation coefficient

Damping ratio: Given that the cantilever beam is a continuum, Eq. (1) describes the time and length of the cantilever. This study only focused on the first-order model vibration characteristics at the cantilever end. Therefore, Eq. (1) and the natural angular frequency ω_i in Eq. (2) can be simplified as follows: D_1 and D_2 are two constants under the first vibration model.

$$w = D_1 \cos \omega_i t + D_2 \sin \omega_i t \quad (8)$$

$$\omega_i = \frac{\lambda_1^2}{l^2}\sqrt{\frac{EI_Y}{\rho A}} \quad (9)$$

According to Eqs. (8) and (9), we can simplify the vibration at the end of the cantilever beam to a particle model, as shown in Fig. 1 (b). The equivalent mass of the specimen is $m = \rho A l$, the equivalent elastic coefficient is $k = \frac{\lambda_1^4 EI_Y}{l^3}$, and c denotes the attenuation coefficient. Therefore, the damping rate of the cantilever beam can be expressed by the following equation:

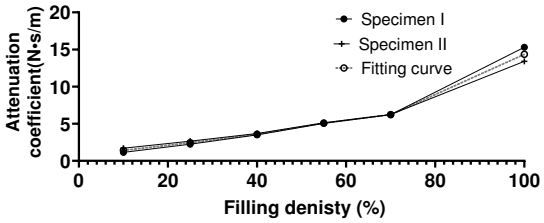

Fig. 6. The attenuation coefficient of Onyx in different filling density.

$$\zeta = \frac{c}{2\sqrt{mk}} = \frac{c}{2\sqrt{\frac{m\lambda_1^4 EI_Y}{l^3}}} \quad (10)$$

The value of the attenuation coefficient c is determined by the material itself; however, c is not a constant and is easily affected by the density of the material. To estimate the damping ratio of the specimen for each filling density, we combined Eqs. (3) and (10) to obtain Eq. (11) to calculate the attenuation coefficient c for each filling density.

The weight m of specimens I, II and the value of the damping ratio are shown in Table. I, II.

$$c = 4m\pi f_i \zeta \quad (11)$$

Fig. 6 shows the variation curve of the attenuation coefficient c for specimens I, II and filling density μ. It can be seen that the attenuation coefficient c increases with the filling density, and the c values of both specimens are similar. The variation in this function is close to that of an exponential function. Similar to the values of EI_Y, we averaged the $c$values of c for each filling density and obtained a fitting curve represented by the dotted line. Similar to Eq. (6), we used the least squares method to derive the equation for the fitting curve of filling density μ and attenuation coefficient c in Fig. 6, as expressed in Eq. (12).

$$c = 1.2381e^{2.453\mu} \quad (12)$$

D. Estimating damping ratio

By combining Eqs. (5), (12) into (10), we can obtain Eq. (13). At this point, we can use Eqs. (7) and (13) to calculate the natural frequency and damping ratio of the robotic arm specimen filled with rectangle pattern and onyx material for any size and filling density.

$$\zeta = \frac{1.2381e^{2.453\mu}}{\sqrt{\frac{m\lambda_1^4(E_s(\frac{BH^3}{12} - \frac{bh^3}{12}) + (-1.47\mu^2 + 3.67\mu - 0.22)(\mu \frac{bh^3}{12}))}{l^3}}} \quad (13)$$

III. EXPERIMENT

To verify the accuracy of Eqs. (7) and (13) for estimating the natural frequency and damping ratio, in addition to comparing specimens I, II, we also selected two specimens of different sizes to compare their estimated and real values of natural frequency and damping ratio. The sizes of the four tested specimens are presented in Table. III, IV.

Fig. 7 shows the experimental device. The specimen was fixed on the vibrator with a fixture and vibrated in the Z-axis direction at a frequency in the range of 10–500 HZ. The

TABLE III

Sizes of 4 specimens

Specimen	I	II	III	IV
$B(mm)$	40	40	45	50
$H(mm)$	20	20	18	15
$b(mm)$	38.4	38.4	43.4	48.4
$h(mm)$	19	19	17	14
$l(mm)$	250	174	200	200

TABLE IV

Weight m of 4 specimens in different filling density

	Mass m (g)			
$\mu(\%)$	I	II	III	IV
10	36.5	22.29	27.56	26.35
25	56.09	36.77		
40	78.43	51.20	63.53	59.44
55	100.40	65.65		
70	122.97	80.13	99.59	92.55
100	166.44	104.53	129.90	120.25

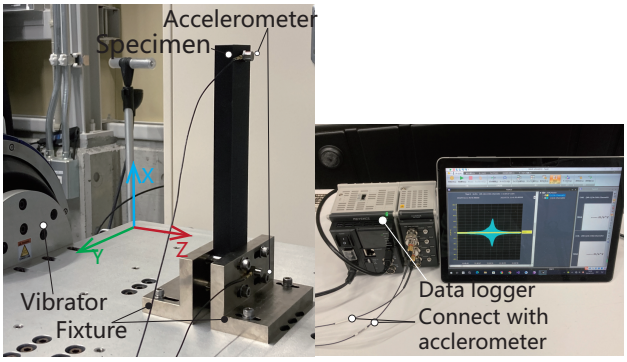

Fig. 7. The experiment device.

specimens were constructed using the Markforged Mark 2 printer. The laminate direction was that of the Z-axis.

Two accelerometers were mounted on the fixture and at the end of the specimen. The data logger entered the acceleration data obtained by the two accelerometers into the PC, and the ratio was calculated. Given that the damping ratio of the specimen was less than 0.1, we used the half-power method [5] to obtain the damping ratio and natural frequency.

A. Comparison of estimated natural frequencies with actual values

Fig. 8 compares the estimated and real frequency values for each specimen; the solid line represents the measured values of natural frequency whereas the dotted line represents the values calculated using Eq. (7).

Fig. 8 shows that the values of natural frequency obtained by Eq. (7) is close to the measured value. As the filling density increased, the natural frequency first decreased and then increased, reaching a minimum around 40%.

B. Comparison of estimated damping ratio with actual values

Fig. 9 compares the estimated and real values of the damping ratio of each specimen; the solid line represents the measured values of damping ratio whereas the dotted line represents the values calculated using Eq. (13).

The estimated curves are close to the measured damping ratios. Note that the damping ratio for all the specimens tested in this study increased slightly with the filling density. The estimated curves reflect this well.

Whether it is the filling density or the damping ratio, the real values of specimens III, IV are approximately consistent with the predicted values, even for different sizes not used in the calculations of the estimated curve. This confirms the accuracy of the proposed Eqs. (7) and (13).

C. Settling time [15]

We aim to use the proposed equations to estimate the optimal filling density before printing. However, it is difficult to determine the optimal filling density based on the natural frequency and damping ratio alone. Therefore, we incorporate the settling time from the occurrence to cessation of vibration as a basis to calculate the filling density with the best anti-vibration effect.

We considered the specimen of a robotic arm that moves with a certain acceleration. We simulated the addition of a weight to the end of the arm. As shown in Fig. 10 (a), when the robotic arm suddenly stopped or started to move, an instantaneous force was applied to the end of the robotic arm.

We regarded the specimen as a particle system, and the elastic coefficient of the equivalent spring k_s was calculated using the following equation:

$$k_s = m(2\pi f)^2 \tag{14}$$

Fig. 10 (b) shows the particle model at the end of the robot arm. The force F at the end of the specimen under instantaneous acceleration a is expressed by the following equation, where F can be divided into the force F_1 generated by the mass of the specimen m under this acceleration. Assuming that an object is carried at the tip of the robot arm, the mass of the object is M, and its inertial force is F_2.

In the initial stage of vibration, we assumed the end velocity of the specimen to be 0, and according to Hooke's law, the initial vibration displacement w_1 of the specimen is as follows:

$$w_1 = \frac{(F_1 + F_2)}{k_s} = \frac{(ma + Ma)}{m(2\pi f)^2} \tag{15}$$

The attenuation of the vibration of the particle system w can be expressed by the following equation:

$$w = w_1 e^{-\zeta \omega t} \sin(\omega_d t + \phi) \tag{16}$$

where, ϕ is the initial phase, we assumed it was $-\frac{\pi}{2}$, and ω_d is the damping natural angular frequency. At each maximum vibration amplitude, the sin value is ± 1. We set the acceleration a applied at the end of the specimen as 15 m/s^2.

As indicated by Fig. 11, the end of the specimen vibrates in the range of $\pm w_1 e^{-\zeta \omega t}$. We define the time t_{th} required for the amplitude w to decrease below w_{th} as the settling time. The settling time t_{th} can be calculated using the following equation

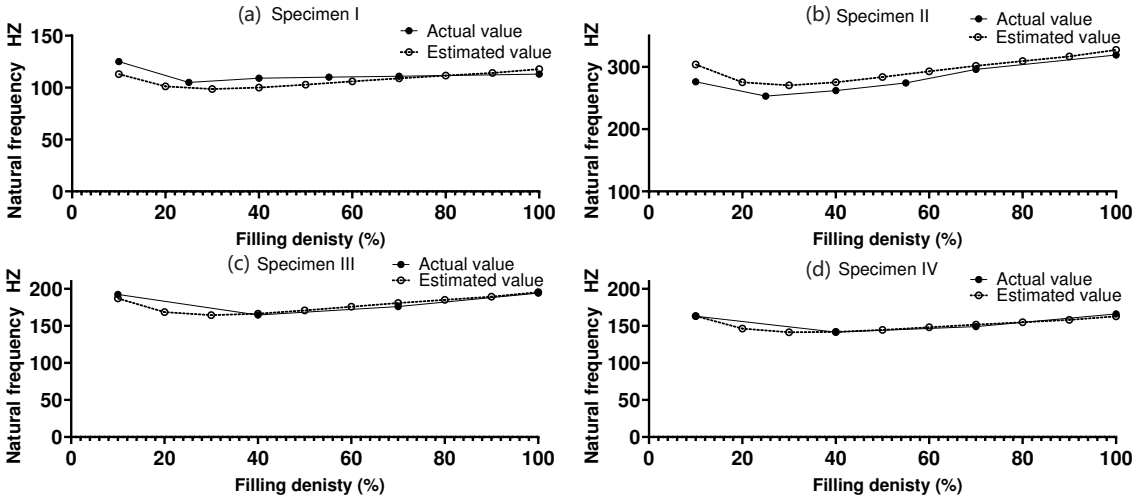

Fig. 8. Comparison of estimated natural frequencies with actual values.

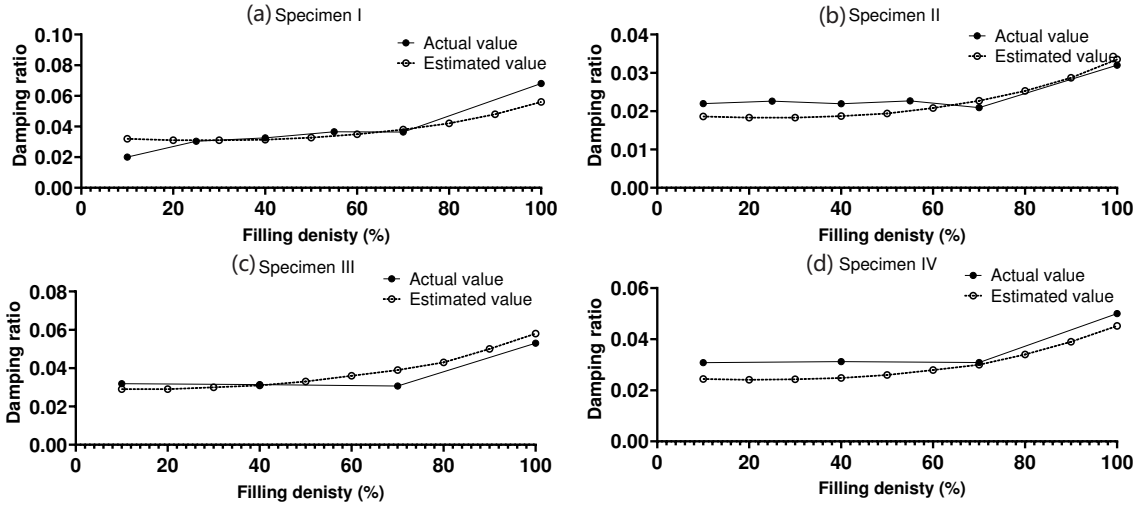

Fig. 9. Comparison of estimated damping ratio with actual values.

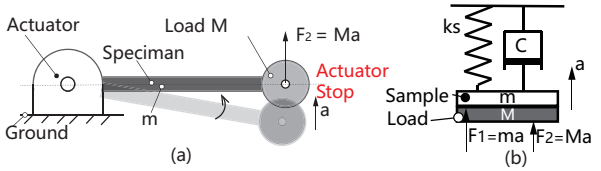

Fig. 10. (a) Simulated robot arm. (b) Load robot arm particle model.

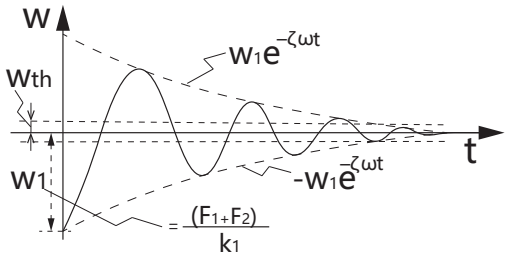

Fig. 11. Peak of damping vibration.

$$t_{th} = \frac{-ln\frac{w_{th}}{w_1}}{\zeta\omega} = \frac{-ln\frac{2\pi m f^2 w_{th}}{Ma+ma}}{2\zeta\pi f} \tag{17}$$

We set the vibration displacement w_{th} of the specimen to 0.02 mm when the vibration of the specimen approximately stopped. In previous studies, we found that under low-end load, a lower filling density leads to a shorter settling time owing to a smaller inertia force generated by the self-weight m. Under a high-end load, the specimen with high filling density exhibits higher stiffness, and the settling time becomes shorter. The optimal filling density varies with the end load. Thus, we set two different end loads M: 0.02 kg and 5 kg.

Substituting the estimated natural frequency and damping ratio obtained from Eq. (7) and (13) into Eq. (17), the estimated settling time is compared with the settling time obtained from the natural frequency and damping ratio ob-

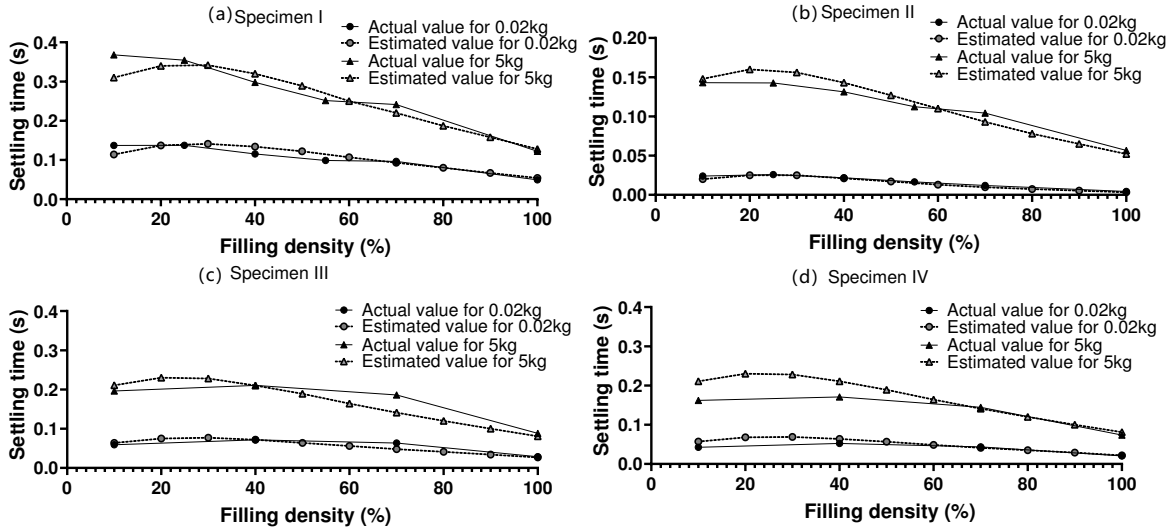

Fig. 12. Comparison of estimated settling time with actual values.

tained from actual experiments.

Fig. 12 shows that the prediction curve can be employed for accurately calculating the settling time of the robot arm specimen under different end loads. Regardless of the size of the end load, the settling time increases first and then decreases with the filling density, reaching a maximum in the range of 25%- 30%. This means that when the filling density in this area is used to construct the robot arm, the anti-vibration effect is the worst and should be avoided.

Note that when the end load of the robot arm specimen with a filling density of 10% is light, the settling time becomes comparable to that of the robot arm with a filling density of 70%. When the end load is heavy, the settling time is greater than that of many other specimens featuring high filling density.

According to the specimens tested, when the filling density exceeds 70%, a shorter settling time is obtained and the minimum is obtained for a filling density of 100%. The real values of the settling time also follow this trend, confirming the effectiveness of the proposed prediction curve. Using the proposed equations and curves, guidelines can be provided to design a robot arm with a certain anti-vibration effect.

IV. CONCLUSIONS AND DISCUSSION

In this study, we measured the natural frequency and damping ratio of onyx-material robot arm specimens. We experimentally measured the variation law of the Young's modulus and attenuation coefficient of the onyx material with the filling density. Based on it, we obtained the equations for estimating the natural frequency and damping ratio of robot arm specimens of any size and filling density. Then, we explored how to determine the optimal filling density under different loads.

Both the estimated and real values of the settling time show that the shockproof effect of the specimens is the worst for a filling density of 25-30%. Therefore, this filling density should be avoided. Secondly, the settling time for a 10% filling density is shorter than that of many specimens with a high filling density. To achieve light weights, a 10% filling density may be an option. For a filling density greater than 70%, no matter how the load at the end varies, the settling time continues to decrease, reaching its minimum at 100%. The proposed equations and curves can provide guidelines to design a robot arm with a certain anti-vibration effect.

In the future, we will adjust the filling pattern and design the internal structure to develop additional design standards that enhance the vibration resistance of 3D-printed robotic arms.

ACKNOWLEDGMENT

This research is subsidized by New Energy and Industrial Technology Development Organization (NEDO) under a project JPNP20016. This paper is one of the achievements of joint research with and is jointly owned copyrighted material of ROBOT Industrial Basic Technology Collaborative Innovation Partnership. We thank Prof. Gen Endo (Tokyo Institute of Technology), Prof. Yusuke Ohta (Chiba Institute of Technology), and Naoyuki Takesue (Tokyo Metropolitan University) for their valuable comments and discussion.

REFERENCES

[1] T. Takaki, M Kanekiyo, G Endo, Damping Characteristics in Adaptation of Plastics for Robot Structures, 2023 IEEE/SICE International Symposium on System Integration(SII), January 17-20, 2023.

[2] K. Wang, X. Xie, J. Wang, A. Zhao, Y. Peng, Y. Rao, Effects of infill characteristics and strain rate on the deformation and failure properties of additively manufactured polyamide-based composite structures, Results in Pyhsics, 18 (2020), 103346.

[3] C. Abeykoon, P. Sri-Amphorn, A. Fernando, Optimization of fused deposition modeling parameters for improved PLA and ABS 3D printed structures, International Journal of Lightweight Materials and Manufacture, March 2020, DOI: 10.1016/j.ijlmm.2020.03.003.

[4] Onyx: Alailable from: https://markforged.com/jp/materials.

[5] Y. Bao, T. Takaki, Influence of 3D Printing Filling Density on Vibra tion Characteristics of Robot Structure, 2024 IEEE/SICE International Symposium on System Integration (SII).

[6] K. Osawa, G. Endo, Does Thin-Walled Metal Pipe Insertion Increase the Bending Strength of 3D Printed Parts?, 2024 IEEE/SICE Interna tional Symposium on System Integration (SII).